Journal for ImmunoTherapy of Cancer

Implication of ^{99m}Tc-sum IL-2 SPECT/CT in immunotherapy by imaging of tumor-infiltrating T cells

Yu Gao,[1] Qi Luo,[2] Zhichen Sun,[1] Hannan Gao,[1] Yue Yu,[1] Yining Sun,[1] Xiaotu Ma,[1] Chuanhui Han,[3] Jiyun Shi ,[1] Fan Wang [1,2,3]

To cite: Gao Y, Luo Q, Sun Z, *et al*. Implication of ^{99m}Tc-sum IL-2 SPECT/CT in immunotherapy by imaging of tumor-infiltrating T cells. *Journal for ImmunoTherapy of Cancer* 2023;**11**:e005925. doi:10.1136/jitc-2022-005925

► Additional supplemental material is published online only. To view, please visit the journal online (http://dx.doi.org/10.1136/jitc-2022-005925).

YG and QL contributed equally. JS and FW contributed equally.

Accepted 12 February 2023

[1]Key Laboratory of Proteinand Peptide Pharmaceuticals, CAS Center for Excellence in Biomacromolecules, Institute of Biophysics Chinese Academy of Sciences, Beijing, China
[2]Guangzhou Laboratory, Guangzhou, China
[3]Medical Isotopes Research Center and Department of Radiation Medicine, State Key Laboratory of Natural and Biomimetic Drugs, School of Basic Medical Sciences, International Cancer Institute, Peking University, Beijing, China

Correspondence to
Professor Fan Wang; wangfan@bjmu.edu.cn

Dr Jiyun Shi; shijiyun@ibp.ac.cn

ABSTRACT

Background Although immune checkpoint blockade (ICB) and adoptive T cell transfer (ACT) therapy have achieved impressive clinical outcomes, majority of patients do not respond to immunotherapy. Tumor-infiltrating T cells, a critical factor to immunotherapy, is dynamically changing. Therefore, a reliable real-time in vivo imaging system for tumor-infiltrating T cells, but not immunohistochemical analyses, will be more valuable to predict response and guide immunotherapy. In this study, we developed a new SPECT/CT imaging probe ^{99m}Tc-sum IL-2 targeting the IL-2Rβ/IL-2Rγ (CD122/CD132) receptor on tumor-infiltrating T cells, and evaluated its application in predicting the immune response to anti-PD-L1 (αPD-L1) therapy as well as tracking infused T cells in ACT therapy.

Methods The binding affinity of the super mutated IL-2 (sum IL-2) in various T cell subtypes was measured. Sum IL-2 was subsequently labeled with ^{99m}Tc through Sortase-A mediated site-specific transpeptidation. SPECT/CT imaging and biodistribution studies of ^{99m}Tc-sum IL-2 were performed in a MC38 mouse model. Wild type IL-2 (IL-2) was used as control in the above studies. Finally, we evaluated ^{99m}Tc-sum IL-2 SPECT/CT for the detection of tumor-infiltrating T cells in the context of αPD-L1 immunotherapy and ACT therapy.

Results Sum IL-2 preferentially bound to CD8$^+$ T cells, especially activated CD8$^+$ T cells, while IL-2 showed biased binding to Treg cells. As a result, ^{99m}Tc-sum IL-2 could detect tumor-infiltrating T cells. In the MC38 tumor model, SPECT/CT imaging showed the increased tumor uptake of ^{99m}Tc-sum IL-2 after αPD-L1 treatment, suggesting that the treatment significantly increased tumor-infiltrating T cells, resulting in a correspondingly significant curative effect. In addition, ^{99m}Tc-sum IL-2 SPECT/CT could also track the infiltration of antigen-specific cytotoxic CD8$^+$ T cells during ACT therapy.

Conclusion ^{99m}Tc-sum IL-2 has great clinical potential for non-invasive and specific SPECT/CT imaging of tumor-infiltrating T cells as well as for timely prediction and evaluation of the therapeutic efficacy of ICB and ACT therapy.

WHAT IS ALREADY KNOWN ON THIS TOPIC

⇒ Tumor-infiltrating T cells, especially activated CD8$^+$ T cells, are vital to immunotherapies, and positively corelate with the prognosis, thus a reliable method for in vivo monitoring of tumor-infiltrating T cells has important clinical values.

WHAT THIS STUDY ADDS

⇒ IL-2-based tracers, such as [^{18}F]FB-IL-2 and ^{99m}Tc-IL-2, have been in clinical trials, but the binding affinity of IL-2 to immunosuppressive Treg cells is much stronger than to CD8$^+$ T cells, making them less reliable in assessing immunotherapy responses. In this study, a novel tracer ^{99m}Tc-sum IL-2 was developed, which preferentially bound to activated CD8$^+$ T cells rather than Treg cells, therefore, ^{99m}Tc-sum IL-2 SPECT/CT showed great potential for predicting immunotherapy response and assessing immunotherapy efficacy in clinical practice.

HOW THIS STUDY MIGHT AFFECT RESEARCH, PRACTICE OR POLICY

⇒ Since non-invasive nuclear imaging can provide real time, in vivo, dynamic, comprehensive, and quantitative information, monitoring the dynamic distribution of T cells in vivo before and during treatment by ^{99m}Tc-sum IL-2 SPECT/CT may help to guide the immunotherapy and improve the therapeutic effect for immune checkpoint blockade and adoptive T cell transfer therapy.

BACKGROUND

In the past decades, immunotherapies, especially immune checkpoint blockade (ICB) and adoptive T cell transfer (ACT) therapy, have made remarkable progress, but only function in a minority of certain patients with cancer.[1–4] Tumor-infiltrating T cells, vital to immunotherapies,[5] positively corelate with the prognosis.[6–8] Therefore, monitoring the dynamic distribution of T cells in vivo before and during treatment may help to guide the immunotherapy and improve the therapeutic effect. Additionally, these are also useful to reflect dynamic change of local and systemic immune responses and help to develop novel immunotherapies.

The current clinical methods used to detect T lymphocytes in whole blood[9] or heterogeneous tumor biopsies[10] do not reflect the dynamic spatiotemporal distribution of T

lymphocytes. In addition, antitumor therapies might influence T cell proliferation and localization throughout the body.[11 12] Non-invasive nuclear imaging can provide real time, in vivo, dynamic, comprehensive, and quantitative information.[13] It thus has high potential to become an integral tool for guiding immunotherapy.

In 1998, the US Food and Drug Administration approved interleukin-2 (IL-2), a classic cytokine that specifically binds and amplifies T cells, to treat patients with stage IV (metastatic) melanoma. There are three subunits of IL-2 receptors (IL-2Rs), IL-2Rα (CD25), IL-2β (CD122), and IL-2γ (CD132), which are highly expressed on the surface of T cells.[14] IL-2Rs have two forms, IL-2Rαβγ (trimer) and IL-2Rβγ (dimer).[14] Treg cells highly express IL-2Rαβγ, while naïve $CD8^+$ T cells, $CD4^+/CD8^+$ T cells and NK cells highly express IL-2Rβγ.[15] Wild-type IL-2 shows higher binding affinity to IL-2Rαβγ than IL-2Rβγ (Kd values 10^{-11} vs 10^{-9} M), therefore, IL-2 preferentially binds to immunosuppressive Treg cells over tumor-killing $CD8^+$ T cells.[16] Sum IL-2 is an artificial variant of IL-2 with six mutations, while L80F, R81D, L85V, I86V and I92F mutations enhance the binding affinity to IL-2Rβ; and F42A mutation reduces the interaction with IL-2Rα.[17] Therefore, sum IL-2 preferentially binds to tumor-infiltrating cytotoxic T cells. In this study, we developed a novel single photon emission computed tomography (SPECT) tracer, ^{99m}Tc-sum IL-2, and evaluated its application in predicting the immune response to anti-PD-L1 (αPD-L1) therapy as well as tracking infused T cells in ACT therapy.

METHODS

Cells and animal models

MC38 cells were obtained from the Cell Resource Center, Peking Union Medical College (which is the headquarters of the National Infrastructure of Cell Line Resource, NSTI, Beijing, China). MC38-ovalbumin (MC38-OVA) and CTLL-2 cells were kindly provided by the lab of Prof. Yangxin Fu at the Institute of Biophysics, Chinese Academy of Sciences (Beijing, China). Cells were cultured in 5% CO_2 at 37°C and maintained in high-glucose Dulbecco's modified Eagle's medium (DMEM) or RPMI-1640 supplemented with 10% heat-inactivated fetal bovine serum (FBS). All cell lines were routinely tested using a mycoplasma contamination kit (R&D). Female C57BL/6 and BALB/c nu/nu mice were purchased from Vital River Laboratory Animal Technology (Beijing, China). Foxp3-GFP mice (BALB/c background) and C57BL/6-Tg (TcraTcrb)1100Mjb/Crl (OT-I) mice were kindly provided by the lab of Prof. Yangxin Fu. MC38 cells (5×10^5) were inoculated subcutaneously (s.c.) into the right hind leg or front flanks of C57BL/6 mice. The animals were randomly used for in vivo studies when the tumor size reached 80-150 mm^3. MC38 cells are a murine colon cancer line, while MC38-OVA cells are derived from MC38 cells expressing the OVA protein. All mice were maintained under specific pathogen-free conditions in the animal facility of the Institute of Biophysics. Animal care and experiments were carried out under institutional protocols and guidelines.

Protein expression and purification

The human wild-type IL-2 (IL-2: APTSSSTKKTQLQLEH LLLDLQMILNGINNYKNPKLTRMLTFKFYMPKKATE LKHLQCLEEELKPLEEVLNLAQSKNFHLRPRDLISN INVIVLELKGSETTFMCEYADETATIVEFLNRWITF CQSIISTLTGGGGSDSLEFIASKLAGSLPETGGSHH HHHHHHHH) and IL-2 variant (sum IL-2: APTSSSTK KTQLQLEHLLLDLQMILNGINNYKNPKLTRMLT**A** KFYMPKKATELKHLQCLEEELKPLEEVLNLAQSKNFH **FD**PRD**VV**SNINV**F**VLELKGSETTFMCEYADETATIVE FLNRWITFCQSIISTLTGGGGSDSLEFIASKLAGSLPETG GSHHHHHHHHHH) with LPETG-tag and histidine tag (His-tag) were expressed and purified from *Spodoptera frugiperda* (Sf9) cells (insect cells), as previously described.[18] Briefly, Sf9 cells were used to generate high-titer recombinant virus expressing the recombinant protein and were cultured at 28°C using SF900 II SFM medium (Invitrogen). Full-length IL-2 (residues 1–133) with a C-terminal histidine tag was cloned into the pFastbac1 vector. After expression, the proteins were purified by Ni column (Cytiva), concentrated using Centricon (Millipore) spin concentrators and purified with an HPLC Superdex-75 sizing column (Increase 10/300 GL, GE Healthcare Life Science).

The detail information of bioassay of sum IL-2 was shown in online supplemental material.

Preparation of ^{99m}Tc-sum IL-2

The two-step site-specific labeling approach was adopted for preparation of ^{99m}Tc-sum IL-2 as previously described.[19] First, GGGGK-HYNIC peptide (GGGGK=Gly-Gly-Gly-Gly-Lys, HYNIC=6-hydrazinonicotinyl) was labeled with ^{99m}Tc. Subsequently, GGGGK-HYNIC-^{99m}Tc was conjugated with an LPETG tag on sum IL-2 with penta-mutant Sortase-A. His-tagged Sortase-A and unreacted sum IL-2 were removed by an Ni column (Cytiva). The product was further purified by high-performance size exclusion chromatography (Superdex^{TM}75 column increase 10/300 GL, GE Healthcare Life Science) using phosphate buffer saline (PBS) (pH 7.4) as the eluent. The radiochemical purity of ^{99m}Tc-sum IL-2 was determined using instant thin layer chromatography-silica gel (Agilent, USA) developed in saline. The stability of ^{99m}Tc-sum IL-2 was evaluated by adding 50 µL of tracer to 450 µL of mouse serum. The mixture was vortexed and incubated at 37°C for 4 hours. After incubation, radiochemical purity was determined by an HPLC assay. The preparation of ^{99m}Tc-IL-2 was the same as ^{99m}Tc-sum IL-2.

In vivo evaluation of ^{99m}Tc-sum IL-2

For small-animal SPECT/CT imaging, each MC38 tumor-bearing mouse was injected via the tail vein with 18.5 MBq of ^{99m}Tc-sum IL-2 or ^{99m}Tc-IL-2 (n=4). The blocking study was also performed in MC38 tumor-bearing mice (n=3) by intratumor injection of 100 µg sum IL-2 prior

to intravenous injection of ^{99m}Tc-sum IL-2 at 18.5 MBq. At 0.5 hour after injection, mice were anesthetized by inhalation of 2% isoflurane and imaged using a nanoScanSPECT/CT (Mediso, Hungary) following a standard protocol. The pinhole SPECT images (peak, 140 keV; 20% width; frame time, 25 s) were acquired for 13.5 min, and CT images were subsequently acquired (50 kVp; 0.67 mA; rotation, 210°; exposure time, 300 ms). All SPECT images were reconstructed and further analyzed with Fusion (Mediso) by drawing volumes of interest on the tumor and major organs.

For the biodistribution study, each MC38 tumor-bearing mouse was injected with 0.37 MBq of radiotracer via the tail vein and sacrificed at 0.5 hour after injection (n=4/group). Blood, tumors, and organs of interest were harvested, weighed, and counted. The radioactivity in the tissues was measured using a γ-counter. The results are presented as the percentage of injected dose per gram of tissue (%ID/g). Blocking biodistribution studies were also performed in MC38 tumor-bearing mice (n=4). Here, each mouse was intravenously co-injected with 100 µg of unlabeled sum IL-2 and 0.37 MBq of ^{99m}Tc-sum IL-2. At 0.5 hour post-injection (p.i.), all mice in the blocking group were sacrificed, and the organ biodistribution of the radiotracer was determined.

For the intratumor T cell uptake assay, tumor-bearing mice were injected intravenously with 18.5 MBq of ^{99m}Tc-sum IL-2. The mice were euthanized, and tumors were collected 0.5 hour after radiotracer administration. Tumors were chopped and digested in DMEM with DNase I (Sigma-Aldrich) and collagenase IV (Sigma-Aldrich) at 37°C for 1 hour on a shaking platform with the speed of 200 rpm. Single cell suspension was obtained through a 70 µm filter. The cells were resuspended in MACS buffer (PBS+2% FBS + 2 mM EDTA) and counted. Then, $CD4^+$ and $CD8^+$ T cells were fractionated using serial magnetic bead positive selection according to the manufacturer's instructions (Miltenyi Biotec). In brief, cells were resuspended at 10 million total cells per 90 µL of MACS buffer and 10 µL of microbeads for 0.5 hour. Then, the cell suspensions were applied to LS columns in Miltenyi QuadroMACS Separators, washed and eluted according to the manufacturer's instructions. Fractions were resuspended in 1 mL of medium; 10 µL was used for cell counting, approximately 50 µL was stained for flow cytometry determination of fraction cellular composition, and 900 µL was transferred into 5 mL tubes to measure radioactivity.

^{99m}Tc-sum IL-2 SPECT/CT for imaging immune responses during αPD-L1 therapy

When the average diameter of tumors reached approximately 5 mm, tumor-bearing mice were intravenously injected with ^{99m}Tc-sum IL-2 for SPECT/CT imaging and biodistribution studies (n=4). From 1-day post-SPECT/CT scanning, tumor-bearing mice receive 12.5 mg/kg αPD-L1 antibody (clone 10F.9G2; BioXCell) treatment three times at 4-day intervals (n=8), while tumor-bearing mice without treatment were used as controls (n=6). One day after the second αPD-L1 treatment, 4 mice per group were injected with ^{99m}Tc-sum IL-2 again for SPECT/CT imaging and biodistribution study, and tumor infiltration of T cells was analyzed by flow cytometry.

Implication of ^{99m}Tc-sum IL-2 SPECT/CT in ACT therapy

BALB/c nu/nu mice were s.c. injected with either 5×10^5 MC38 or MC38-OVA cells into the right or left flanks, respectively. When the tumors were approximately 5 mm in diameter, tumor-bearing mice were injected with ^{99m}Tc-sum IL-2 for SPECT/CT imaging and biodistribution studies as baseline controls (n=4). One day after SPECT/CT scanning, the tumor-bearing mice received 1×10^7 spleen cells from OT-I mice and were challenged with 50 µg of OVA via intraperitoneal injection 1 day later. On day 2 after cell transfer, mice were subjected to SPECT/CT imaging and biodistribution studies.

Statistical analysis

Numerical results are reported as the mean±SD. Means were compared using Student's t-test with Prism V.8.0 (GraphPad Software, USA). p values less than 0.05 were considered to indicate significance.

RESULTS

Production and functional characterization of sum IL-2

The sum IL-2 was prepared with a yield of 3 mg/L and purity >95% (figure 1A). The molecular weight of sum IL-2 (~20 kDa) was consistent with the calculated molecular mass of sum IL-2 (online supplemental figure S1).

Sum IL-2 showed strong biological activity, with an EC_{50} value of 12.8 pM (online supplemental figure S2). The binding affinity of sum IL-2 to human IL-2Rα was significantly lower (undetectable) than that of IL-2 (EC_{50}=13.5 nM) (figure 1B). In contrast, the affinity of sum IL-2 to human IL-2Rβ was strikingly higher than that of IL-2 (EC_{50}=21.2 nM vs 1138 nM) (figure 1B). Thereby, sum IL-2 preferentially bound to $CD8^+$ T cells, especially activated $CD8^+$ T cells, while IL-2 showed biased binding to Treg cells but not activated $CD8^+$ T cells (figure 1C; online supplemental figure S3). Similarly, sum IL-2 also showed enhanced binding affinity to activated $CD4^+$ T cells compared with IL-2 (online supplemental figure S3).

Preparation of ^{99m}Tc-sum IL-2

^{99m}Tc-sum IL-2 was subjected to site-specific radiolabeling by Sortase-A (figure 2A). The overall labeling yield for ^{99m}Tc-sum IL-2 was >50% and the radiochemical purity was >95% after purification (figure 2B). Additionally, ^{99m}Tc-sum IL-2 was stable in mouse serum, with >90% of the tracer remaining intact after 4-hour incubation (online supplemental figure S4).

In vivo evaluation of ^{99m}Tc-sum IL-2

SPECT/CT imaging showed strong radioactivity accumulation of ^{99m}Tc-sum IL-2 in the MC38 tumors with a clear background at 0.5 h p.i. High renal uptake indicated that

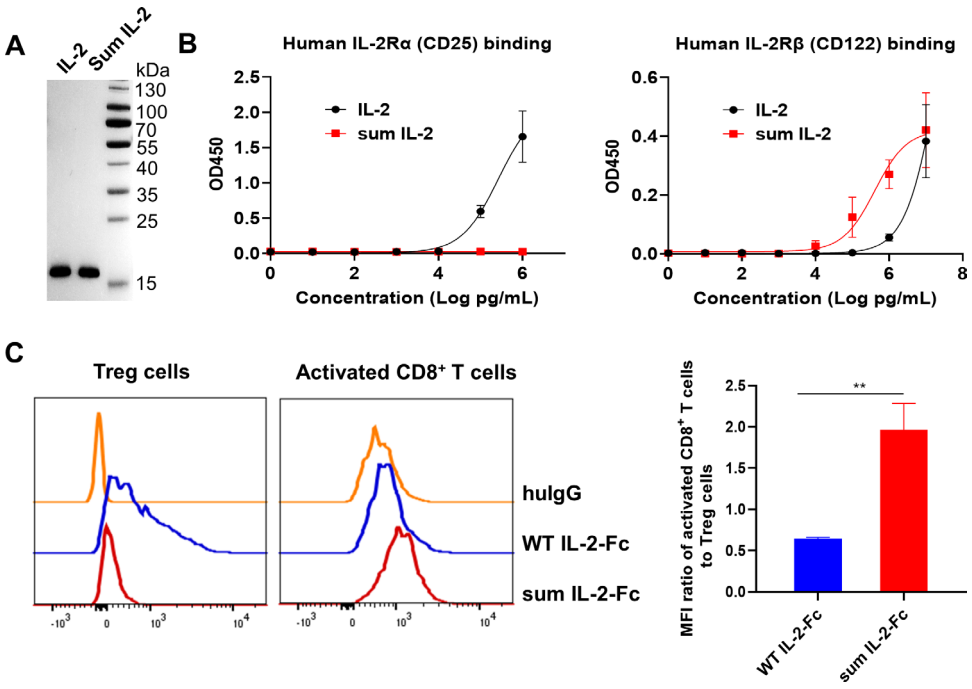

Figure 1 In vitro characterization of sum IL-2 and IL-2. (A) SDS-PAGE of IL-2-LPETG-10*His and sum IL-2-LPETG-10*His. (B) ELISA was used to detect the binding of IL-2 and sum IL-2 to the human IL-2 receptor α subunit or β subunit. (C) flow cytometric detection of the binding of IL-2 and sum IL-2 to $CD3^+CD8^+CD44^{high}$ activated T cells and $CD3^+CD4^+Foxp3^+$ Treg cells in the mouse spleen. **p<0.01. SDS-PAGE, sodium dodecyl sulfate polyacrylamide gel electrophoresis; MFI, mean fluorescence intensity.

the probe was metabolized mainly through the urinary system (figure 3A). In the blocking imaging, intratumoral injection of excessive sum IL-2 significantly reduced the signal of ^{99m}Tc-sum IL-2 in the tumor (figure 3A). Biodistribution study confirmed the decrease of tumor uptake (2.67±0.10 vs 1.97±0.11 %ID/g; p<0.01) at 0.5 hour p.i. (figure 3B), suggesting the uptake of ^{99m}Tc-sum IL-2 in tumors was specifically mediated. Notably, ^{99m}Tc-sum IL-2 was also aggregated in T-cell enriched spleen and tumor-draining lymph node (TdLN) (6.57±0.21 and 3.71±0.24 %ID/g) (figure 3B). Excess cold sum IL-2 reduced the uptake of ^{99m}Tc-sum IL-2 in spleen and

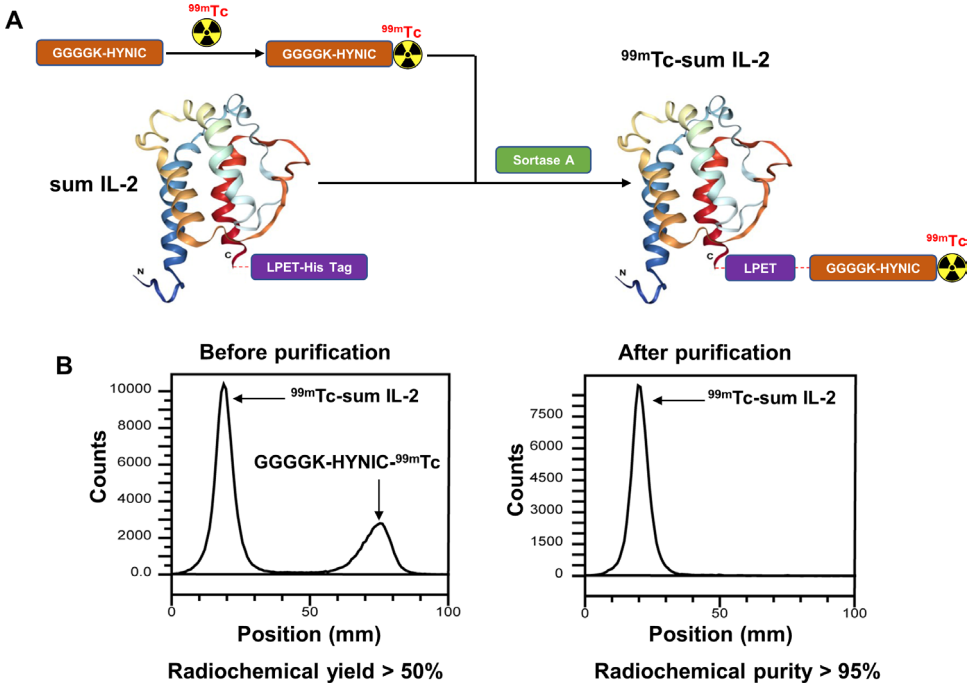

Figure 2 Radiochemistry of ^{99m}Tc-sum IL-2. (A) Radiolabeling procedure for ^{99m}Tc-sum IL-2. (B) ITLC chromatograms of the ^{99m}Tc-sum IL-2 before and after purification. ITLC, instant thin layer chromatography.

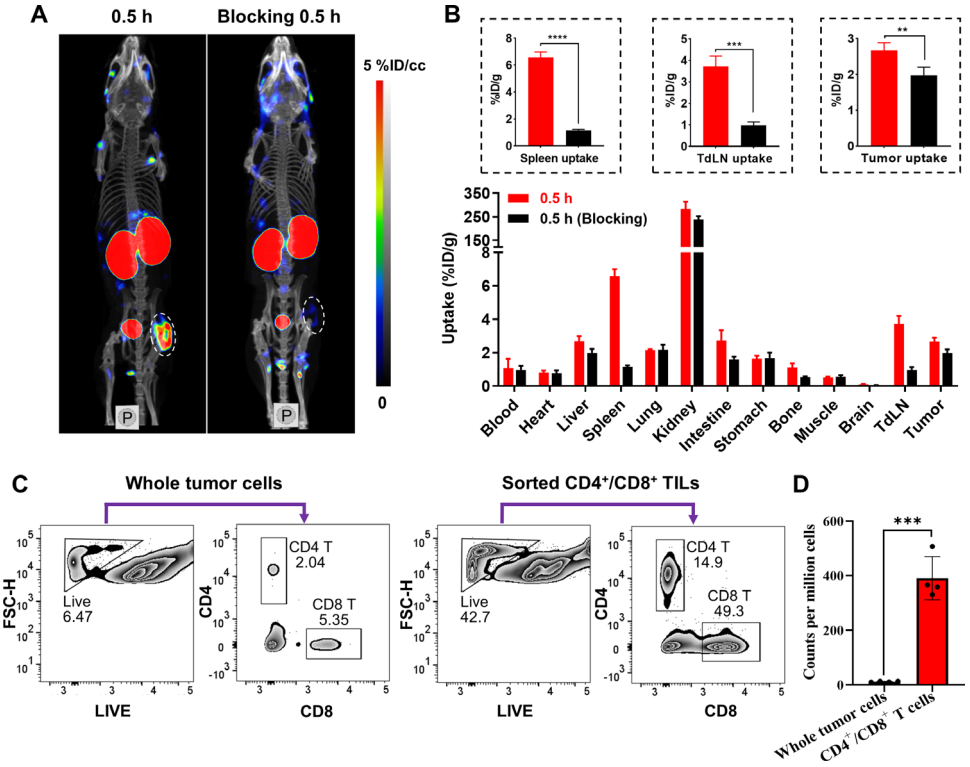

Figure 3 ^{99m}Tc-sum IL-2 specifically detects T cells in vivo. (A) Representative small animal SPECT/CT images obtained after injection of ^{99m}Tc-sum IL-2 in MC38 subcutaneous tumor-bearing mice without or with blocking doses of sum IL-2 protein. (White dashed circle indicates the tumor) (B) Biodistribution of ^{99m}Tc-sum IL-2 in MC38 tumor-bearing mice, as well as a blocking study performed by co-injecting ^{99m}Tc-sum IL-2 and cold sum IL-2 protein (n=4/group). **p<0.01, ****p<0.001. (C) Representative flow cytometry analysis of the MC38 whole tumor, CD8$^+$ and CD4$^+$ T cell fractions. (D) ^{99m}Tc-sum IL-2 avidity in designated cell fractions from MC38 tumors (n=4/group). All the experiments were carried out twice. SPECT, single photon emission computed tomography; FSC-H, Forward Scatter Hight; TdLN, tumor-draining lymph node.

TdLN (1.15±0.04and 0.98±0.08 %ID/g, p<0.001) (figure 3B), indicating that the uptake of ^{99m}Tc-sum IL-2 in spleen and TdLN was a specific uptake associated with T cells. Although the blockage of tumor uptake was not as pronounced as in the spleen and lymph nodes, this might be because after injection of cold sum IL-2 through the tail vein, most of it was exhausted in the spleen and lymph nodes, resulting in the greatly reduced amount of IL-2 reaching the tumors, thus the uptake of tumors could not be deeply blocked. When the cold sum IL-2 was injected peritumorally in the imaging blocking experiment, the blockage of tumor uptake was relatively more thorough.

To address whether ^{99m}Tc-sum IL-2 specifically bound to T cells in the tumor microenvironment (TME), the tumor-infiltrating CD4$^+$/CD8$^+$ T cells were isolated using magnetic microbeads and compared with whole tumor cells (figure 3C). The results showed that the uptake of ^{99m}Tc-sum IL-2 per million cells in tumor-infiltrating CD4$^+$/CD8$^+$ T cells (390.74±79.26 Counts) was significantly higher than that in unfractionated whole tumor cells (11.87±1.68 Counts) (p<0.001) (figure 3D), indicating that ^{99m}Tc-sum IL-2 preferentially bound to tumor-infiltrating CD4$^+$/CD8$^+$ T cells in the TME.

^{99m}Tc-sum IL-2 is superior to ^{99m}Tc-IL-2 in imaging of tumor-infiltrating T cells

As shown in figure 4A,B, tumor uptake of ^{99m}Tc-sum IL-2 at 0.5-hour p.i. was significantly higher than that of ^{99m}Tc-IL-2 (2.67±0.10 vs 2.04±0.09 %ID/g, p<0.01), indicating that ^{99m}Tc-sum IL-2 was more specific than ^{99m}Tc-IL-2 to detect tumor-infiltrating T cells in the immune-responsive MC38 tumor model. In addition, the uptake of ^{99m}Tc-sum IL-2 in the T-cell enriched spleen and TdLN was also higher than that of ^{99m}Tc-IL-2 (spleen: 6.57±0.21 vs 5.29±0.26 %ID/g, p<0.01; TdLN: 3.71±0.24 vs 2.66±0.09 %ID/g, p<0.05) (figure 4B).

^{99m}Tc-sum IL-2 SPECT/CT imaging for the assessment of ICB

We then evaluated whether ^{99m}Tc-sum IL-2 could trace the dynamic change of tumor-infiltrating T cells induced by αPD-L1 treatment (figure 5A). As shown in figure 5B, αPD-L1 treatment markedly increased uptake of ^{99m}Tc-sum IL-2 in tumors. Biodistribution study confirmed the significant increase of ^{99m}Tc-sum IL-2 uptake in tumors of αPD-L1-treated mice (3.62±0.29 %ID/g) compared with untreated mice (2.48±0.25 %ID/g, p<0.01), indicating an effective system immunity response promoted by αPD-L1 treatment (figure 5C). Besides the tumors, αPD-L1 treatment also increased uptake of ^{99m}Tc-sum

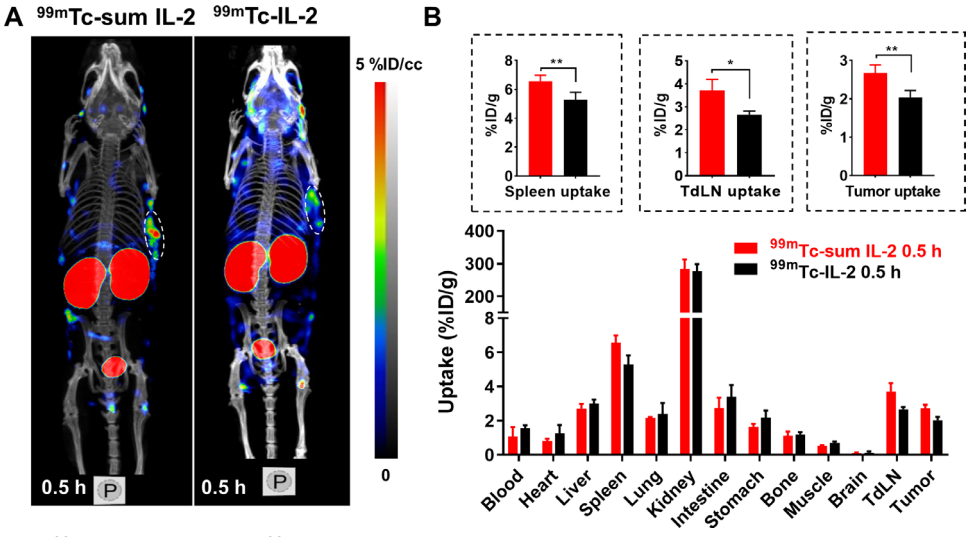

Figure 4 Comparison ^{99m}Tc-sum IL-2 and ^{99m}Tc-IL-2. (A) Representative small animal SPECT/CT images obtained at 0.5 hour after injection of ^{99m}Tc-sum IL-2 or ^{99m}Tc-IL-2 in MC38 subcutaneous tumor-bearing mice (white dashed circles indicate tumors). (B) Biodistribution of ^{99m}Tc-sum IL-2 or ^{99m}Tc-IL-2 in MC38 tumor-bearing mice at 0.5 h p.i. TdLN (n=4/group). All the experiments were carried out twice. *p<0.05, **p<0.01. SPECT, single photon emission computed tomography; TdLN, tumor-draining lymph node.

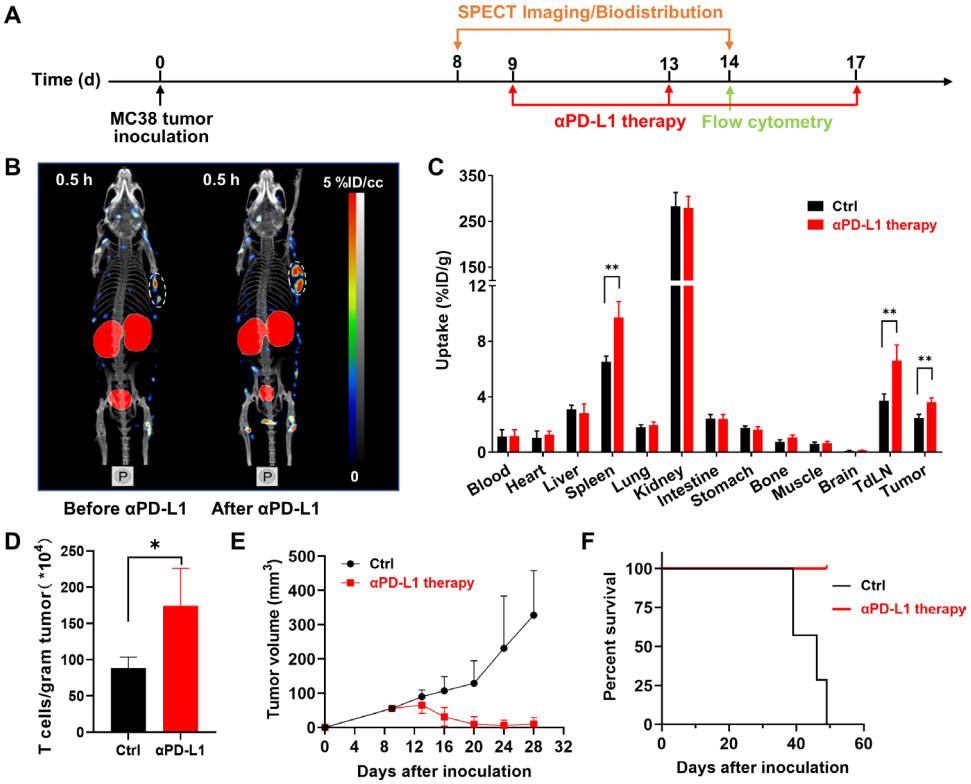

Figure 5 ^{99m}Tc-sum IL-2 SPECT/CT imaging and biodistribution of MC38 tumor-bearing mice receiving αPD-L1 therapy. (A) C57BL/6 mice bearing s.c. MC38-tumors were treated with αPD-L1 therapy three times (day 9, 13 and 17) and ^{99m}Tc-sum IL-2 SPECT/CT imaging and biodistribution were acquired before treatment (day 8) and after second αPD-L1 treatment (day14), flow cytometry performed at day 14. (B) SPECT/CT imaging in MC38 models before and after αPD-L1 treatment. (White dashed circles indicate tumors) (C) Biodistribution of ^{99m}Tc-sum IL-2 in αPD-L1-treated or untreated mice at 0.5 h p.i. (n=4/group). **p<0.01. (D) Flow cytometry analysis of tumors was used to determine the number of $CD45^+CD3^+$ T cells in the MC38 tumors in αPD-L1-treated and untreated mice (n=4/group). *p<0.05. (E) Tumor growth curves (mean±SD) (n=6-8/group) and (F) Kaplan-Meier survival curves (n=6-8/group). All the experiments were carried out twice. SPECT, single photon emission computed tomography; Ctrl, control; p.i, post-injection; s.c., subcutaneously; TdLN, tumor-draining lymph node.

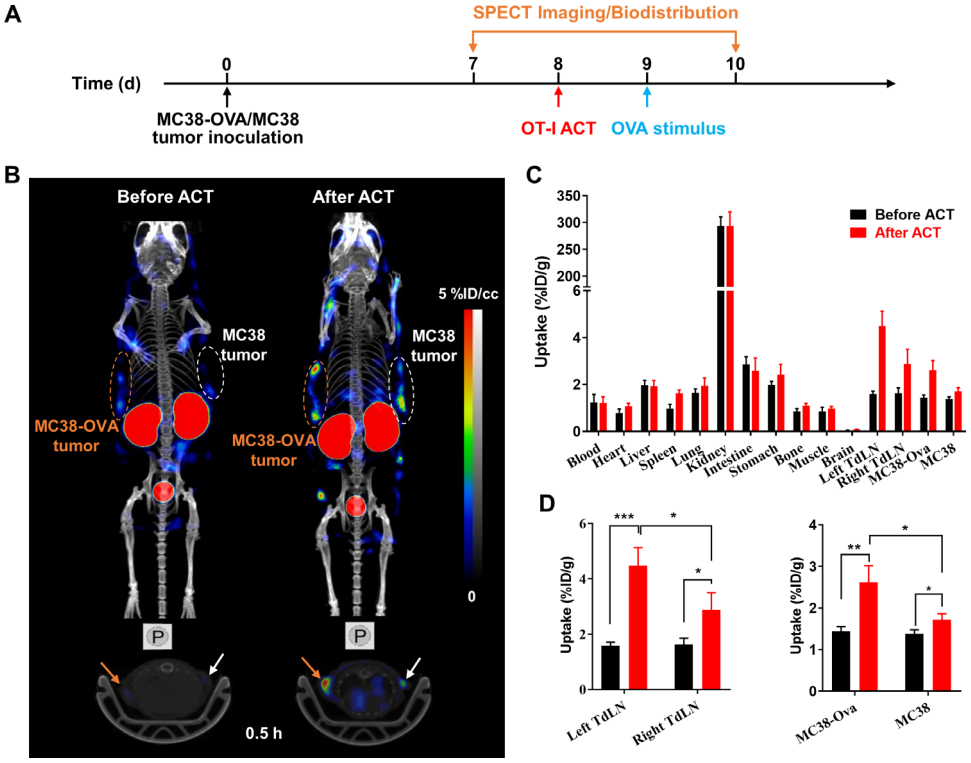

Figure 6 ^{99m}Tc-sum IL-2 SPECT/CT imaging and biodistribution in the OT-I adoptive T cell therapy MC38 tumor model. (A) C57BL/6 mice bearing s.c. MC38-OVA/MC38 tumors were treated with OT-I ACT and ^{99m}Tc-sum IL-2 SPECT/CT imaging and biodistribution were acquired before and after ACT. MC38 and MC38-OVA tumor cells were subcutaneously injected in the right and left flank of BABL/c nu/nu mice. One day after adoptive OT-I T cell transfer, OVA protein was intraperitoneally injected in BABL/c nu/nu mice. (B) SPECT/CT images at 0.5 hour after injection of ^{99m}Tc-sum IL-2 in BABL/c nu/nu mice bearing MC38-OVA and MC38 tumors before transfer and 2 days after adoptive OT-I T cell transfer. (Brown dashed circles and arrows indicate MC38-OVA tumors; white dashed circles and arrows indicate MC38 tumors) (C) Biodistribution of ^{99m}Tc-sum IL-2 in control and T cell transferred mice bearing MC38-OVA and MC38 tumors at 0.5 h p.i. (n=4/group). (D) Comparative analysis of ^{99m}Tc-sum IL-2 uptake in tumor and TdLN before and after ACT. *p<0.05, **p<0.01, ***p<0.001. SPECT, single photon emission computed tomography; ACT, adoptive T cell transfer; OVA, ovalbumin; s.c., subcutaneously; p.i., post-injection; TdLN, tumor-draining lymph node.

IL-2 in T-cell enriched spleen (9.71±1.17 vs 6.52±0.41 %ID/g, p<0.01) and TdLN (6.60±1.14 vs 3.71±0.48 %ID/g, p<0.01) (figure 5C). Consistently, αPD-L1 treatment significantly increased the infiltrated T cells in tumors (174.54±51.57 vs 88.58±14.80 (×10^4) T cells/gram tumor, p<0.05) (figure 5D). Accordingly, MC38 tumors responded well to αPD-L1 treatment, and 100% of treated mice showed significantly robust and durable tumor eradication compared with untreated controls (p<0.001) (figure 5E,F).

In vivo imaging of adoptively transferred T cells

To investigated ^{99m}Tc-sum IL-2 for tracing the dymanic infiltration of T cells in ACT, we examined homing of OVA-specific $CD8^+$ T cells (OT-I cells) to MC38-OVA tumors after ACT by ^{99m}Tc-sum IL-2 SPECT/CT imaging (figure 6A). As shown in figure 6B–D, the MC38-OVA and MC38 tumors showed similar uptake of ^{99m}Tc-sum IL-2 before ACT (1.44±0.11 vs 1.38±0.10 %ID/g), and both two were significantly increased after ACT (2.62±0.40 vs 1.44±0.11 %ID/g, p<0.01; 1.72±0.15 vs 1.38±0.10 %ID/g, p<0.05), but the uptake in MC38-OVA tumors was increased notably more than that in MC38 tumors (2.62±0.40 vs 1.72±0.15 %ID/g, p<0.05). In addition, the TdLN of MC38-OVA and MC38 mice were also showed significantly increased uptake of ^{99m}Tc-sum IL-2 after ACT (1.59±0.12 to 4.48±0.65 %ID/g, p<0.001; 1.63±0.23 to 2.88±0.63 %ID/g, p<0.05), and the uptake in MC38-OVA TdLN was increased much more than that in MC38 TdLN (4.48±0.65 vs 2.88±0.63 %ID/g, p<0.05) (figure 6C,D).

DISCUSSION

T cell-based tumor immunotherapy has become a powerful tool against cancer, but only a small fraction of patients with advanced solid tumors has objective responses to it. Up to now, the mechanism why the majority of patients do not respond to immunotherapy is still unclear, however, compelling evidence suggests that robust intratumoral T lymphocyte infiltration is a critical component of successful immunotherapy.[6–8] Current methods of assessing tumor-infiltrating T cells by tumor biopsy are invasive and may not always be practical or available. Furthermore, due to tumor immunological heterogeneity, the level of tumor-infiltrating T cells determined by biopsy may not represent the actual

status.[20] A non-invasive imaging method capable of accurately assessing T cell infiltration in tumors would be very useful in the clinic to better determine the effectiveness of treatments.

Many T cell imaging tracers are undergoing preclinical research, including $CD8^+$ or $CD4^+$ T cell targeting antibodies and diabody or engineered antibody fragments,[21–24] OX40 (or CD134) targeting ^{89}Zr-DFO-OX40 mAb,[25] CD25 (IL-2α receptor) preferentially binding [^{18}F]FB-IL-2[26] and ^{99m}Tc-IL-2,[27 28] cytoplasmic deoxycytidine kinase and deoxyguanosine kinase targeting [^{18}F]F-AraG,[29] and lymphocyte activation gene-3 (LAG-3) targeting ^{99m}Tc-LAG-3 nanobody.[30] These strategies have shown promise for predicting the response to immunotherapy in preclinical studies. Among them, IL-2-based tracers have been used in clinical trials, but the binding affinity of IL-2 to immunosuppressive Treg cells is much stronger than to $CD8^+$ T cells, making them less reliable in assessing immunotherapy responses.[14] Especially, ^{18}F-IL-2 was reported as a tool for non-invasive PET imaging of $CD25^+$ (IL-2Rα) activated T cells in patients received ICB therapy, but its uptake in tumors was relatively low due to the low expression of CD25 detected in tumor tissues. In addition, it could not reliably reflect treatment-related immune responses, because the upregulation of IL-2Rα on T cells after ICB treatment is transient, and IL-2Rα expression in tumors is mainly limited to immunosuppressive Treg cells rather than activated CD8 T cells.[31] The sum IL-2, as a biased IL-2 mutant, not only reduced its binding to IL-2Rα subunits and greatly reduced its binding to Treg cells, but also increased its binding to the IL-2β subunit, which enhanced its ability to detect activated $CD4^+$ T cells and $CD8^+$ T cells, especially activated $CD8^+$ T cells. Therefore, radiolabeled sum IL-2 can provide reliable and sensitive means to detect intratumor effector T cells for predicting the prognosis of immunotherapy in clinical practice.

Previously, ^{18}F- or ^{99m}Tc-labeled wild-type IL-2 were all prepared by non-specific-site labeling methods,[26 32] whose homogeneity and reproducibility are difficult to control. In addition, non-specific-site labeling may affect the binding of IL-2 to T cells. Here, we engineered a flexible GGGGS chain-linked LPETG motif at the C-terminal of sum IL-2, which can be coupled with radiolabeled GGGGK-HYNIC-^{99m}Tc in a site-specific manner by Sortase A, far from the binding site of sum IL-2 to IL-2R to avoid affecting the binding affinity between ^{99m}Tc-sum IL-2 and IL-2Rs. As a result, site-specifically labeled ^{99m}Tc-sum IL-2 showed a lower liver background than previous non-specifically labeled IL-2,[26 33] allowing for the better contrast.

To serve as an immune-monitoring agent, ^{99m}Tc-sum IL-2 must be able to reflect the response to immunotherapy in a timely manner. The longitudinal imaging of mice before and after αPD-L1 treatment clearly demonstrated the ability of ^{99m}Tc-sum IL-2 to detect dynamic increase of tumor-infiltrating T cells. Accordingly, the MC38 tumor model showed a robust response to checkpoint inhibition, leading to significantly improved survival. ^{99m}Tc-sum IL-2 SPECT/CT imaging revealed great promise to predict the response to checkpoint blockade therapy for the further clinical translation.

ACT therapy is based on the infusion of a large number of tumor antigen-specific T cells.[34] Direct radiolabeling of T lymphocytes in vitro allows monitoring of the initial cell migration of adoptively transferred cells but suffers from the limitations of radionuclide half-life, probe signal dilution due to cell division and potential toxic effects of the radionuclide on radiosensitive lymphocytes.[35 36] ^{99m}Tc-sum IL-2 SPECT/CT imaging is a suitable method for non-invasive and specific monitoring of T cells without the need for ex vivo manipulation of lymphocytes. Since OVA expression in syngeneic tumors greatly increased antigen-specific T cell infiltration, we observed a significant increase of OT-I cells in MC38-OVA tumors as well as in ipsilateral TdLN after ACT by the in vivo imaging. The results clearly indicated that ^{99m}Tc-sum IL-2 SPECT/CT imaging could specifically detect tumor-specific T cells infused in the MC38-OVA tumors, which showed good clinical application prospects in ACT efficacy assessment.

CONCLUSION

In this study, a novel tracer, ^{99m}Tc-sum IL-2, was developed to support specific SPECT/CT imaging of tumor-infiltrating T cells in vivo. ^{99m}Tc-sum IL-2 preferentially bound to activated $CD8^+$ T cells rather than Treg cells, and showed selective accumulation in tumor, as well as T-cell enriched spleen and TdLN. Moreover, ^{99m}Tc-sum IL-2 could reflect the dynamic change of tumor-infiltrating T cells in the context of ICB and ACT. This novel tracer showed great potential for predicting immunotherapy response and assessing immunotherapy efficacy in clinical practice.

Acknowledgements We thank Dr. Xiaoda Li at Healthy Analytical Center at Peking University (Beijing, China) for his help with nanoScanSPECT/CT imaging. We especially appreciate the lab of Professor Yangxin Fu at the Institute of Biophysics, Chinese Academy of Sciences (Beijing, China) for kindly providing MC38-OVA and CTLL-2 cells, Foxp3-GFP mice (BALB/c background) and C57BL/6-Tg (TcraTcrb)1100Mjb/Crl (OT-I) mice.

Contributors YG mainly completed the expression, purification, identification and evaluation of sum IL-2 protein, as well as other biological and immunological experiments. QL mainly completed the establishment of radioactive labeling methods and in vivo imaging. Their contributions were of equal importance and therefore joint first authors. Senior authors JS and FW jointly proposed and funded the project, co-directed the experiments, jointly supervised the overall study, as well as wrote and revised the manuscript. The former focuses on chemical research such as labeling, while the latter pays more attention to biological research. Their contributions are equally important. ZS, HG, YY, YS, and XM helped with in vivo experiments; CH helped with statistical analysis and paper revision; FW is acting as a guarantor. All authors contributed to the writing and approval of the final manuscript.

Funding This work was supported in part by the National Natural Science Foundation of China (NSFC) projects (92159201, 81630045, 81971676 and 81927802), Emergency Key Program of Guangzhou Laboratory (EKPG21-16).

Competing interests None declared.

Patient consent for publication Not applicable.

Ethics approval All animal experiments were performed in accordance with the Institutional Animal Care and Use Committee (IACUC) at the Institute of Biophysics, Chinese Academy of Sciences and Peking University. The Ethic Committee approval code is LA2021296.

Provenance and peer review Not commissioned; externally peer reviewed.

Data availability statement All data relevant to the study are included in the article or uploaded as online supplemental information.

ORCID iDs
Jiyun Shi http://orcid.org/0000-0001-7220-9637
Fan Wang http://orcid.org/0000-0002-4166-5776

REFERENCES

1 Couzin-Frankel J. *Cancer immunotherapy*. American Association for the Advancement of Science, 2013.
2 McDermott D, Lebbé C, Hodi FS, *et al*. Durable benefit and the potential for long-term survival with immunotherapy in advanced melanoma. *Cancer Treat Rev* 2014;40:1056–64.
3 Ferris RL. Immunology and immunotherapy of head and neck cancer. *J Clin Oncol* 2015;33:3293–304.
4 Doroshow DB, Sanmamed MF, Hastings K, *et al*. Immunotherapy in non-small cell lung cancer: facts and hopes. *Clin Cancer Res* 2019;25:4592–602.
5 Gooden MJM, de Bock GH, Leffers N, *et al*. The prognostic influence of tumour-infiltrating lymphocytes in cancer: a systematic review with meta-analysis. *Br J Cancer* 2011;105:93–103.
6 Leffers N, Gooden MJM, de Jong RA, *et al*. Prognostic significance of tumor-infiltrating T-lymphocytes in primary and metastatic lesions of advanced stage ovarian cancer. *Cancer Immunol Immunother* 2009;58:449–59.
7 Horne ZD, Jack R, Gray ZT, *et al*. Increased levels of tumor-infiltrating lymphocytes are associated with improved recurrence-free survival in stage 1A non-small-cell lung cancer. *J Surg Res* 2011;171:1–5.
8 Fu Q, Chen N, Ge C, *et al*. Prognostic value of tumor-infiltrating lymphocytes in melanoma: a systematic review and meta-analysis. *Oncoimmunology* 2019;8:1593806.
9 Clay TM, Hobeika AC, Mosca PJ, *et al*. Assays for monitoring cellular immune responses to active immunotherapy of cancer. *Clin Cancer Res* 2001;7:1127–35.
10 Otoshi T, Nagano T, Tachihara M, *et al*. Possible biomarkers for cancer immunotherapy. *Cancers (Basel)* 2019;11:935.
11 Lanzavecchia A. Identifying strategies for immune intervention. *Science* 1993;260:937–44.
12 Waldman AD, Fritz JM, Lenardo MJ. A guide to cancer immunotherapy: from T cell basic science to clinical practice. *Nat Rev Immunol* 2020;20:651–68.
13 Zhou Z, Lu Z-R. Molecular imaging of the tumor microenvironment. *Adv Drug Deliv Rev* 2017;113:24–48.
14 Malek TR, Castro I. Interleukin-2 receptor signaling: at the interface between tolerance and immunity. *Immunity* 2010;33:153–65.
15 Merchant R, Galligan C, Munegowda MA, *et al*. Fine-Tuned long-acting interleukin-2 superkine potentiates durable immune responses in mice and non-human primate. *J Immunother Cancer* 2022;10:e003155.
16 Chinen T, Kannan AK, Levine AG, *et al*. An essential role for the IL-2 receptor in Treg cell function. *Nat Immunol* 2016;17:1322–33.
17 Sun Z, Ren Z, Yang K, *et al*. A next-generation tumor-targeting IL-2 preferentially promotes tumor-infiltrating $CD8^+$ T-cell response and effective tumor control. *Nat Commun* 2019;10:3874.
18 Wang X, Rickert M, Garcia KC. Structure of the quaternary complex of interleukin-2 with its alpha, beta, and gammac receptors. *Science* 2005;310:1159–63.
19 Gao H, Wu Y, Shi J, *et al*. Nuclear imaging-guided PD-L1 blockade therapy increases effectiveness of cancer immunotherapy. *J Immunother Cancer* 2020;8:e001156.
20 Reuben A, Spencer CN, Prieto PA, *et al*. Genomic and immune heterogeneity are associated with differential responses to therapy in melanoma. *NPJ Genom Med* 2017;2:10.
21 Tavaré R, McCracken MN, Zettlitz KA, *et al*. Engineered antibody fragments for immuno-PET imaging of endogenous CD8+ T cells in vivo. *Proc Natl Acad Sci U S A* 2014;111:1108–13.
22 Tavaré R, McCracken MN, Zettlitz KA, *et al*. Immuno-PET of murine T cell reconstitution postadoptive stem cell transplantation using anti-CD4 and anti-CD8 cys-diabodies. *J Nucl Med* 2015;56:1258–64.
23 Tavaré R, Escuin-Ordinas H, Mok S, *et al*. An effective immuno-PET imaging method to monitor CD8-dependent responses to immunotherapy. *Cancer Res* 2016;76:73–82.
24 Rashidian M, Ingram JR, Dougan M, *et al*. Predicting the response to CTLA-4 blockade by longitudinal noninvasive monitoring of CD8 T cells. *J Exp Med* 2017;214:2243–55.
25 Nobashi TW, Mayer AT, Xiao Z, *et al*. Whole-Body PET imaging of T-cell response to glioblastoma. *Clin Cancer Res* 2021;27:6445–56.
26 Hartimath SV, Draghiciu O, van de Wall S, *et al*. Noninvasive monitoring of cancer therapy induced activated T cells using [18F] fb-il-2 PET imaging. *Oncoimmunology* 2017;6:e1248014.
27 Signore A, Annovazzi A, Barone R, *et al*. 99mTc-interleukin-2 scintigraphy as a potential tool for evaluating tumor-infiltrating lymphocytes in melanoma lesions: a validation study. *J Nucl Med* 2004;45:1647–52.
28 Chianelli M, Mather SJ, Grossman A, *et al*. 99mTc-interleukin-2 scintigraphy in normal subjects and in patients with autoimmune thyroid diseases: a feasibility study. *Eur J Nucl Med Mol Imaging* 2008;35:2286–93.
29 Levi J, Lam T, Goth SR, *et al*. Imaging of activated T cells as an early predictor of immune response to anti-PD-1 therapy. *Cancer Res* 2019;79:3455–65.
30 Lecocq Q, Awad RM, De Vlaeminck Y, *et al*. Single-Domain antibody nuclear imaging allows noninvasive quantification of LAG-3 expression by tumor-infiltrating leukocytes and predicts response of immune checkpoint blockade. *J Nucl Med* 2021;62:1638–44.
31 van de Donk PP, Wind TT, Hooiveld-Noeken JS, *et al*. Interleukin-2 PET imaging in patients with metastatic melanoma before and during immune checkpoint inhibitor therapy. *Eur J Nucl Med Mol Imaging* 2021;48:4369–76.
32 Karczmarczyk U, Garnuszek P, Maurin M, *et al*. Investigation of 99mtc-labelling of recombinant human interleukin-2 via hydrazinonicotinamide. *Nucl Med Biol* 2010;37:795–803.
33 D'Alessandria C, di Gialleonardo V, Chianelli M, *et al*. Synthesis and optimization of the labeling procedure of 99mtc-HYNIC-interleukin-2 for in vivo imaging of activated T lymphocytes. *Mol Imaging Biol* 2010;12:539–46.
34 June CH. Adoptive T cell therapy for cancer in the clinic. *J Clin Invest* 2007;117:1466–76.
35 Pittet MJ, Grimm J, Berger CR, *et al*. In vivo imaging of T cell delivery to tumors after adoptive transfer therapy. *Proc Natl Acad Sci U S A* 2007;104:12457–61.
36 Griessinger CM, Kehlbach R, Bukala D, *et al*. In vivo tracking of Th1 cells by PET reveals quantitative and temporal distribution and specific homing in lymphatic tissue. *J Nucl Med* 2014;55:301–7.